Reports

Direct Observation of Structural Defects in Laser-Deposited Superconducting Y-Ba-Cu-O Thin Films

R. RAMESH, D. M. HWANG, T. VENKATESAN, T. S. RAVI, L. NAZAR, A. INAM, X. D. WU, B. DUTTA, G. THOMAS, A. F. MARSHALL, T. H. GEBALLE

The defect structure of in situ pulsed, laser-deposited, thin films of the high–transition temperature superconductor Y-Ba-Cu-O has been observed directly by atomic resolution electron microscopy. In a thin film with the nominal composition $YBa_2Cu_3O_7$ (123), stacking defects corresponding to the cationic stoichiometry of the 248, 247, and 224 compounds have been observed. Other defects observed include edge dislocations and antiphase boundaries. These defects, which are related to the nonequilibrium processing conditions, are likely to be responsible for the higher critical currents observed in these films as compared to single crystals.

THE MOST IMPORTANT QUESTION concerning the potential of the new high–superconducting transition temperature (T_c) cuprate superconductors for large-scale applications is whether there is an intrinsic limitation in their ability to carry large currents with little or no loss at temperatures that are greater than or equal to $T_c/2$. A recent news report (*1*) outlines some of the evidence that is the basis for pessimism. On the other hand, the fact that thin films of $YBa_2Cu_3O_7$ (123) have very high critical currents (*2, 3*) with losses many orders of magnitude less than those exhibited by Cu metal when measured only a few degrees below T_c, is, we believe, convincing proof that there is no intrinsic limitation.

There are several key questions regarding the origin of the high critical currents in these thin films. In earlier work (*4*) the lower critical current (J_c) of ceramic samples was attributed to the presence of grain boundaries. Because these oxide superconductors are type II materials with a very small value of the first critical magnetic field (H_{c1}), a flux lattice, either in the ordered form or in the disordered form, is very likely to exist. Indeed, the flux lattice has been observed in single crystals of $YBa_2Cu_3O_7$ (*5*). Thus, if the thin film is to carry a large critical current, it is essential that the fluxons be pinned. Pinning of the flux lattice can, in general, be accomplished by the introduction of structural defects into the lattice. In the case of Y-Ba-Cu-O thin films, the atomic nature of defects, resulting from the deposition process, is still not known, although structural defects in bulk samples have been characterized by atomic resolution imaging [see, for example, (*6, 7*)].

The atomic structure of defects in thin films is the focus of this report. Defects in typical epitaxial films deposited on single-crystal MgO have been examined with high-resolution transmission electron microscopy (HRTEM) at a resolution of 1.6 Å. These films exhibit a sharp ($\leq$1 K) resistive transition at 88 to 90 K and have critical currents of the order of 10^6 A/cm^2 at 77 K.

Details of the thin-film laser deposition process have been reported elsewhere (*2*). Cross-section samples were prepared and were ion-milled for a few minutes before examination so as to reduce the degradation due to moisture in the atmosphere. High-resolution electron microscopy (HREM) was carried out in the Berkeley Atomic Resolution Microscope (ARM) at a point-to-point resolution of 1.6 Å. HREM images were obtained under conditions close to Scherzer defocus such that the projections of the atomic columns appear black on a white background. Images were obtained within a few minutes of exposure to the electron beam to reduce the beam-induced damage. We verified the interpretation of the experimental images by carrying out simulations, using the MacTempas (*8*) software.

Examination of planar sections of the thin-film samples revealed that these films contained transformation twins. Most of the stacking defects are associated with the layered structure of these oxides. The HREM image in Fig. 1 shows a local region where the $YBa_2Cu_3O_y$ (123) structure is observed. This structural interpretation is confirmed by the simulated image shown in the inset. The most common defect observed is the intergrowth of the $YBa_2Cu_4O_8$ structure, that is, one that has two Cu–O chains rather than one. As shown by Zandbergen *et al.* (*6*), the two Cu–O chains are related by either a 1/2[100] or a 1/2[010] glide symmetry, both of which were observed in this study. This structure was subsequently detected by x-ray diffraction and electron diffraction in thin films of Y-Ba-Cu-O (*9*) and was found to have a T_c of 81 K. In the HREM image in Fig. 2 the 248 structure with the 1/2[010] glide symmetry is presented. The interpretation of the image contrast in terms of the extra Cu–O layer is confirmed by the results of the image simulations, shown in the inset to Fig. 2 for the 1/2[010] shift.

Two other types of stacking defects that were observed are illustrated in Fig. 3. The experimental image in Fig. 3 shows, in addition to the "perovskite block" consisting

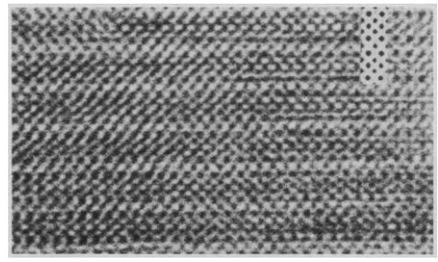

Fig. 1. Atomic resolution image of the [100] zone axis, showing the $YBa_2Cu_3O_7$ (123) structure; inset shows the simulated image for a foil thickness of 20 Å and a defocus of −450 Å, confirming the interpretation of the experimental image.

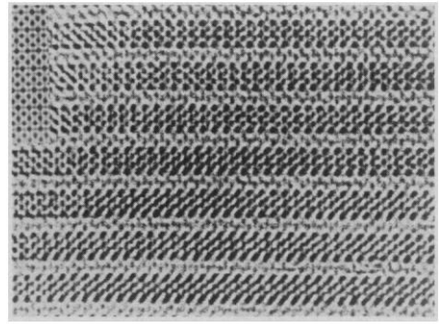

Fig. 2. Atomic resolution image of the [100] zone, revealing the cationic positions of the $YBa_2Cu_4O_8$ (248) structure, in which the two Cu–O layers are related by a 1/2[010] glide; inset shows the simulated image corresponding to the experimental image for a foil thickness of 20 Å and a defocus of −450 Å.

R. Ramesh, D. M. Hwang, T. Venkatesan, T. S. Ravi, L. Nazar, Bellcore, Red Bank, NJ 07701.
A. Inam and X. D. Wu, Rutgers University, Piscataway, NJ 08854.
B. Dutta, Middlebury College, Middlebury, VT 05753.
G. Thomas, Department of Materials Science and Mineral Engineering and National Center for Electron Microscopy, Materials and Chemical Sciences Division, Lawrence Berkeley Laboratory, University of California, Berkeley, CA 94720.
A. F. Marshall and T. H. Geballe, Stanford University, Stanford, CA 94305.

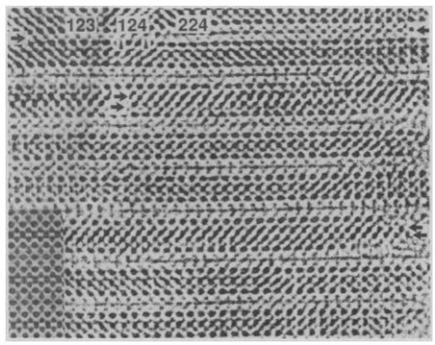

Fig. 3. Atomic resolution of the image [100] zone axis of the $Y_2Ba_2Cu_4O_9$ (224) defect; inset shows the simulated image for a foil thickness of 20 Å and a defocus of −450 Å, confirming the interpretation of the image. Note also two unit cells in which an extra Ba layer is intercalated in the perovskite block (arrows).

of the sequence "BaO–CuO_2–Y–CuO_2–BaO," another unit consisting of three rows of black dots. To identify the cationic species in these sites, we carried out detailed image simulations with different combinations of the cations. The best fit of the experimental image to the simulated image, shown in the inset to Fig. 3, was obtained for the unit consisting of two Cu–O chains between which a Y atom is located with eightfold oxygen coordination. There are four oxygen atoms in the Y plane and two each in the two Cu–O chains above and below the Y layer. The stereochemistry of Y in this site is different from that of the Y ion in the perovskite block. This structure, with the stoichiometry of $Y_2Ba_2Cu_4O_9$, is charge-balanced when the formal charges are used and is likely to be insulating. Because doping and the type of conductivity depend on the O content, there is always the possibility of altering the O content to induce charge carriers and possibly superconductivity in this structure.

The same structure has also been observed as an isolated defect in bulk samples of nominal cationic composition corresponding to 123 (7). Defects in the perovskite block have also been observed (although less frequently than the defects discussed above), one of which is identified by arrows in the structural image in Fig. 3. This unit cell shows a contrast that is different from that of other perovskite blocks. The intensity at this position suggests that an extra Ba layer has been intercalated, which is glide-related to the Y layer. Such a defect has not been reported before in the Y-Ba-Cu-O system.

The lower magnification HREM image in Fig. 4 illustrates the complex intermixed defect structure of these films. This image also shows two antiphase boundaries (APB), planar defects that are frequently observed in these films. On either side of the boundary the film is in the same orientation, that is, [100], but the cationic layers in the two sides are out of phase because of the difference in stacking sequence. In addition, several of the stacking defects described above in Figs. 2 and 3 are intimately mixed in this local region. Transformation of one structure to another takes place by the introduction or the removal of the corresponding cationic layer or layers during growth. In a general sense, this corresponds to the introduction of an edge dislocation with the Burger's vector along the *c* direction. For example, the 123 stacking sequence could be converted into the 224 stacking, Fig. 3, in two stages. First, in a very local region, shown by arrows in Fig. 3, the 248 structure (containing two Cu–O chains) is observed. Subsequently, an extra Y layer appears between the two Cu–O layers of the 248 structure to give the 224 structure. Thus, different polytypoidic variants form in order to accommodate local changes in composition along the *a–b* plane and along the *c* direction.

The larger variety and density of defects found in thin films, as compared to the bulk, is a consequence of the nonequilibrium growth involved in the deposition process. Because only short-range diffusion and atomic rearrangement are permissible under the deposition conditions, the incoming species in the laser plume are "frozen" into a relatively metastable configuration. The basic perovskite block is rarely disturbed. The structural changes take place mainly in the layers between two such units. These layers are also the doping centers in the Y-Ba-Cu-O system, and hence there is a definite possibility of changes in superconducting properties, as exemplified by the 248 structure. The observation of the new stacking sequences in the atomic images also suggests that the relatively nonequilibrium laser deposition process can be used to produce new metastable structures with novel properties. The 224 structure is one such example. The fact that these defects are associated with the layered nature of these cuprates suggests that these defects are likely to be a generic feature of all in situ deposited thin films. Indeed, the defects presented in this report have also been observed in thin films deposited on $SrTiO_3$, although the density of the various defects appears to be different.

The connection between the flux pinning, leading to higher critical currents and smaller magnetic field–induced resistive broadening as compared to what occurs in single crystals, and the defects remains to be established. As in the low T_c superconductors, flux pinning by structural defects, with superconducting properties different from that of the matrix, is likely to play an important role. In the bulk form some of these defects, such as the 248 or the 247 structures, are superconducting with a T_c lower than that of the 123 phase and thus may be suitable pinning sites in the thin films. Although there is no information available on transport properties of the 224 phase, based on formal charge balance considerations, this phase is likely to be insulating and hence may also be a source of flux pinning. The interconversion of the stacking defects along the *a–b* plane to accommodate local changes in composition, could also provide the pinning required to resist vortex motion in the *a–b* plane. More quantitative studies through the control of the defect density are needed to establish the relationships. Ultimately, this will assist in designing superconductors with better transport properties.

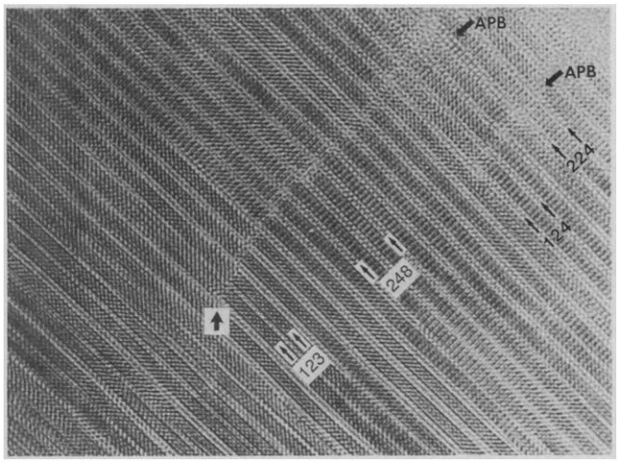

Fig. 4. A typical HREM image of the [100] zone axis, showing the complex intermixed defect structure of the film. The 123, 124, 248, and 224 structures are narrowed. Two antiphase boundaries (APB) are also observable in this image.

REFERENCES AND NOTES

1. R. Pool, *Science* **245**, 931 (1989).
2. See, for example, B. Dutta, X. D. Wu, A. Inam, T. Venkatesan, *Solid State Technol.* **32**, 106 (1989), and the references therein.
3. A. Inam *et al.*, *Appl. Phys. Lett.*, in press.
4. P. Chaudhari, F. K. LeGoues, A. Segmüller, *Science* **238**, 342 (1987).
5. G. J. Dolan, G. V. Chandrasekhar, T. R. Dinger, C.

Field, F. Holtzberg, *Phys. Rev. Lett.* **62**, 827 (1989).
6. H. W. Zandbergen *et al.*, *Nature* **331**, 596 (1988).
7. A. Ourmazd *et al.*, *ibid.* **327**, 308 (1987).
8. MacTempas is a program for the simulation of HRTEM images and is a registered trademark of R. Kilaas, c/o Total Resolution, Berkeley, CA.
9. A. F. Marshall *et al.*, *Phys. Rev. B* **37**, 9353 (1988).
10. We acknowledge stimulating discussions with and the support of P. L. Key, J. H. Wernick, J. M. Tarascon, M. J. Bowden, P. F. Liao, and J. M. Rowell. The assistance of the staff of the National Center for Electron Microscopy is greatly appreciated. The work at Lawrence Berkeley Laboratory is supported by the Director, Office of Energy Research, Office of Basic Energy Sciences, Materials Sciences Division of the U.S. Department of Energy under contract DE-AC03-76SF00098. The work at Stanford University is supported in part by the Center for Materials Research under the National Science Foundation Materials Research Laboratories program.

6 September 1989; accepted 26 October 1989

A Light Source Smaller Than the Optical Wavelength

K. LIEBERMAN, S. HARUSH, A. LEWIS, R. KOPELMAN

A method has been developed for the efficient emission of light from subwavelength dimensions. It is based on packaging photons as molecular excitons, effectively reducing the volume of the light beam by 10^9 and making possible propagation through dimensions of 1 nanometer. Molecular microcrystals are grown in the tips of micropipettes that have inner diameters of 100 nanometers or less. Measurements are presented that demonstrate this improvement in transmission for pipettes of various diameters. The ultrasmall dimensions of these light sources, the wavelength range (ultraviolet to red) of their emission, their ease of production, and their expected unique abilities for high efficiency excitation-imaging of surfaces portend significant applications for this methodology.

RECENTLY THERE HAS BEEN considerable interest in the development of schemes for subwavelength illumination (*1–4*). The aim of most of this research has been to advance near-field light microscopic imaging of surfaces to the resolution of a scanning electron microscope (*2–4*). Indeed, such superresolution light microscopy has enabled researchers to optically examine a variety of specimens without being limited by the diffraction properties of visible light. The basis of this near-field imaging technique is the following. As an electromagnetic wave emerges from an aperture, it is at first highly collimated to the aperture dimension. It is only after the wave has propagated a finite distance from the aperture that the diffraction that limits classical optical imaging takes effect. Thus, in the near-field region, a beam of light is present that is largely independent of the wavelength and is determined solely by the size and shape of the aperture (*5*). A critical factor in such near-field imaging systems is the nature of the light probe that accomplishes the subwavelength illumination. In this report we present an approach for producing sources of light with subwavelength dimensions and with significant improvement over previous approaches. Our method involves aiding the transmission of light through subwavelength dimensions with the introduction of crystals that store light energy as excitons, propagate these excitons in dimensions that are less than 10 nm, and then emit the light in a highly local region of a surface.

Several approaches have been used for producing subwavelength illumination, all of which involve the stopping down of a larger light source with some form of aperture. In one of the more successful methods for producing such subwavelength apertures, a metal-coated glass micropipette has been used that can be produced readily with inner diameters (at the tip) of less than 50 nm (*6, 7*). The details of pipette fabrication have been described elsewhere (*6, 7*). Even though the dimension of these pipettes can be reduced significantly below 50 nm, it has been argued that it would be difficult to reduce the spot size of such a light probe below this diameter. The essence of the argument is that the spot size of such an aperture depends ultimately on the finite conductivity of the metallic coating around the pipette. In order to appreciate this point, one has to remember that there are no propagating electromagnetic modes in a subwavelength cylindrical metallic wave guide such as a metal-coated pipette. The least attenuated mode for a round aperture has been found to be the TE_{11} mode, for which the energy decays at a rate of

$$E = E_0 \exp[-2 \times 1.81(\ell/a)] \quad (1)$$

where ℓ is the length of the aperture and a is the radius (*5*). With a sufficiently rapid tapering of the pipette, however, this evanescent region can be kept short enough to obtain a fairly large throughput of light. In addition to this effect, the electromagnetic wave penetrates the metallic coating and decays within it at a finite rate given by

$$E = E_0 \exp(-d/c) \quad (2)$$

where d is the depth of penetration and c is the extinction length of the metal. When the attenuation due to the wave-guide effect exceeds the attenuation in the metal, the contrast between the aperture and the surrounding medium becomes insufficient for superresolution applications. The metal with the largest opacity in the visible region is aluminum, for which $c = 6.5$ nm when the wavelength is 500 nm. This yields a minimum usable aperture of about 50 nm. In practice, multilayered coatings are necessary to obtain good adhesion and a practical aperture is expected to perform with reduced efficiency.

Our solution makes use of the energy-packaging capabilities of certain materials to circumvent the boundary problem of the edge of the aperture. According to our present understanding of energy propagation in materials, excitations can be confined to molecular and atomic dimensions under appropriate conditions (*8–16*). We have used this property of materials in our development of a subwavelength light source by growing a suitable energy-confining crystal within the subwavelength confines of a pipette. With this approach, energy can be guided directly to the aperture at the pipette tip instead of being allowed to propagate freely in the form of an electromagnetic wave through a region of the pipette whose dimension cannot support a propagating mode. Such energy-confining materials can be excited through either electrical or radiative processes to produce an abundance of excitons that allow light to be effectively transmitted through the "bottleneck" created by the subwavelength dimensions of the tip near the aperture. The excitons can be produced directly at the tip, or they can be generated within the bulk of the material and allowed to diffuse to the tip by an electric dipole (Forster) transfer mechanism (*8–12*). In either case, these excitons will then undergo a radiative decay, producing a tiny source of light at the very tip of the pipette.

The proximity of the metal coating along the outer surface of the pipette does not interfere with the exciton transfer and should actually help to increase the throughput, because the only allowed radiative transition will be for photons emitted along the

K. Lieberman, S. Harush, A. Lewis, Department of Applied Physics, Hebrew University, Jerusalem 91904, Israel.
R. Kopelman, Department of Chemistry, University of Michigan, Ann Arbor, MI 48109.